Preparation and Performance of the Cathode Precursor Ferric Phosphate for Li-ion Battery Facilitated by Impinging Stream

Yang Xiao[1,2], Weihua Pu[1,], Wenbo Wan[1], Yufang Cui[1]*

[1]Institute of Nuclear & New Energy Technology, Tsinghua University, Beijing, 100084, China
[2]College of Chemistry & Materials, South-Central University for Nationalities, Wuhan, Hubei, China
[*]E-mail: puwh@tsinghua.edu.cn

An improved impinging stream reactor (ISR) was developed to synthesize the cathode precursor ferric phosphate by performing the reaction between $Fe(NO_3)_3 \cdot 9H_2O$ and H_3PO_4 with aqueous ammonia as the precipitating agent. The chemical formula for the synthesized product was identified to be $FePO_4 \cdot 3H_2O$ based on the powder X-ray diffraction (XRD), thermogravimetry and differential scanning calorimeter (TG-DSC), and Fourier transform infrared spectrophotometry (FT-IR) measurements. The $FePO_4 \cdot 3H_2O$ particles were amorphous and will change to pure crystalline phase of anhydrous $FePO_4$ after heating treatment in air at 600 ^{o}C for 5 hours. The particle size distribution (PSD) and morphology were characterized by the laser particle size analyzer and scanning electron microscope (SEM), respectively. It was found that the $FePO_4 \cdot 3H_2O$ prepared by ISR particle size is much finer and PSD is much narrower than that by stirred tank reactor (STR). The flow behaviour of both ISR and STR were investigated by determining the residence time distributions (RTD) using an electroconductivity input-response technique with KCl solution as the tracer. Bourne reaction scheme was employed to investigate the micromixing effects in both ISR and STR. The results show that the degrees of backmixing in the two reactors are similar, but the micromixing effect in the former is much better than that in the latter, which accounts for the $FePO_4 \cdot 3H_2O$ produced by ISR possess finer size and narrower PSD. The cell performance test results indicate that the $LiFePO_4/C$ obtained from $FePO_4 \cdot 3H_2O$ produced by ISR can exhibit a better electrochemical property.

1. INTRODUCTION

The key materials for lithium ion battery include cathode, anode, separator and electrolyte. In contrast, the development of cathode material is slower and has become the bottleneck in the development of lithium ion batteries. The olivine-structured lithium iron phosphate $LiFePO_4$ has been investigated extensively as suitable cathode material since the pioneering works of Padhi *et al*. [1].

LiFePO$_4$ has a high voltage plateau (~3.5V vs. Li/Li$^+$) and large theoretical capacity (~170mAh·g^{-1}), as well as lower cost, environmental benignity and excellent thermal safety natures. Due to these advantages, LiFePO$_4$ becomes one of the most promising cathode materials for lithium ion batteries. However, as for LiFePO$_4$, the main challenge is its poor rate capability caused by the low electronic conductivity and slow lithium ion diffusion, which unfortunately prevents it from being used in high power applications [2-7]. Although LiFePO$_4$ powders have been scale-up produced industrially by the high temperature solid-state route, the molar ratio of Li /Fe / P cannot be accurately controlled and the particle size distribution (PSD) is broad. As a result, the batch consistency of the product performance is poor.

Synthetic conditions and electrochemical characters of electrode materials mainly depend on the precursor. A perfect precursor can provide better electrochemical performance of the product. LiFePO$_4$/C obtained from FePO$_4$ precursor has better electrochemical performance than that obtained from α-Fe$_2$O$_3$ or Fe$_3$O$_4$. This primarily owes to the fact that FePO$_4$ contains equimolar ratio of [Fe] and [PO$_4$] as they are in one compound, which makes it easy to synthesize LiFePO$_4$ [8]. FePO$_4$ can be obtained by the dehydration reaction of FePO$_4$·xH$_2$O [9-12]. The FePO$_4$·xH$_2$O particle size and its distribution strongly affect those of LiFePO$_4$, and further influence the electrochemical performance and the batch consistency of LiFePO$_4$. Meanwhile, the particle size and size distribution are governed by the mixing status of raw materials in the reactor. Impinging stream reactor (ISR) with a special flow configuration can improve mixing by strengthening the mass and heat transfer [13]. Chi *et al* [14] have prepared ultra-fine cerium dioxide powders in a ISR.

The aim of the present study is to produce FePO$_4$·xH$_2$O with fine size and narrow distribution by utilizing an improved ISR to perform the precipitation reaction between Fe(NO$_3$)$_3$·9H$_2$O and H$_3$PO$_4$. For sake of comparison, a conventional stirred tank reactor (STR) was also used to carry out the preparation of FePO$_4$·xH$_2$O. The reasons for the difference between the size and PSD of the product synthesized in ISR and that in STR were analyzed by determining the residence time distributions (RTD) and micromixing effects.

2. EXPERIMENTAL

The experimental apparatus developed by authors is shown in Figure 1. All chemicals were provided by Beijing Chemical Reagent Co. and used directly without further purification. The equimolecular solution of ferric nitrate and phosphoric acid was feed. The improved ISR (ISR) with an effective volume of 3.5L is consist of reactor shell, two drawing tubes with baffle plates, two propellers driven by two constant speed motors, two feeding pipes. All experiments of precursor synthesis were carried out in the mode of continuous operation under the conditions as follows, the reaction temperature of 50 °C, reactant initial concentration of 1.0 mol/L, solution pH of 2.30, and stirring speed of 1500 rpm. The stirring speed was controlled precisely by a photoelectric tachometer. A temperature-compensated pH meter (PHSJ-4A, Shanghai) was used to monitor the pH of the reaction system. The pH electrode was calibrated with the buffer solutions of pH 4 and 7, respectively. FePO$_4$ particles should form at acidic solution. In this work, the reaction solution pH was adjusted and

maintained to be 2.30 by slowly adding ammonium hydroxide solution. The reactor jacket was thermostated by heating water using a thermostatic bath. After reaching the steady state conditions, a 10 mL sample was taken to analyze the particle size. The precipitates flowed out of the reactor were collected and washed with deionized water, then dried in a dry oven at 80 $^{\circ}$C for 12 hours.
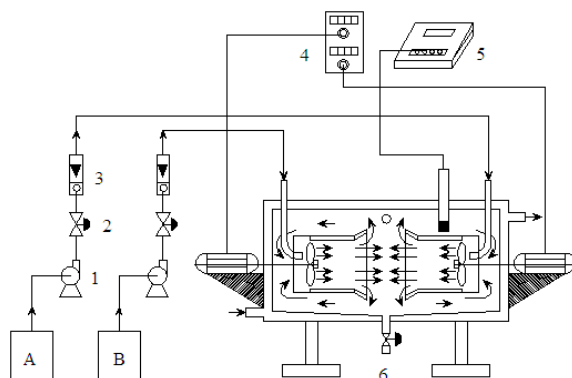

Figure 1. Schematic diagram of impinging stream apparatus: A,B-reservoir;1-pump;2-valve;3-rotameter;4-speed controller;5-pH meter;6-ISR.

The composition and structure of the $FePO_4 \cdot xH_2O$ precursor were characterized by the powder X-ray diffraction (XRD, Bruker D8 Advance), thermogravimetry and differential scanning calorimeter (TG-DSC, STA 449F3,NETZSCH), and Fourier transform infrared spectrophotometry (FT-IR, Spectrum GX FTIR system) measurements. The particle size and the morphology were characterized by the laser particle size analyzer (LS13320/ULM2, Beckman) and scanning electron microscope (SEM, Hitachi S-5500), respectively.

In order to measure the electrochemical performance of the cathode material $LiFePO_4$, the procedures of the lithiation of $FePO_4$, the preparation of the working electrodes and the assembly of experimental cell were described in detail later (see 3.5).

3. RESULTS AND DISCUSSION

3.1. Particle structure

Figure 2 shows the XRD patterns of the the as-prepared precipitate without further treatment and that after being calcined at different temperatures for 5 hours. As the same as the results reported by Refs. [9,15], it can be observed that the untreated particles are amorphous since the XRD profiles did not show any diffraction peaks. This amorphous structure is held nearly up to 500 $^{\circ}$C. When the sintering temperature exceeds 500 $^{\circ}$C, a transformation from amorphous to a crystalline phase occurs and a series of diffraction peaks appear. All the detectable peaks of the synthesized powders sintered at 600 $^{\circ}$C are consistent with the characteristic XRD peaks of $FePO_4$ (PDF card number 29-0715), indicating that the general formula of the as-prepared precipitate is $FePO_4 \cdot xH_2O$.
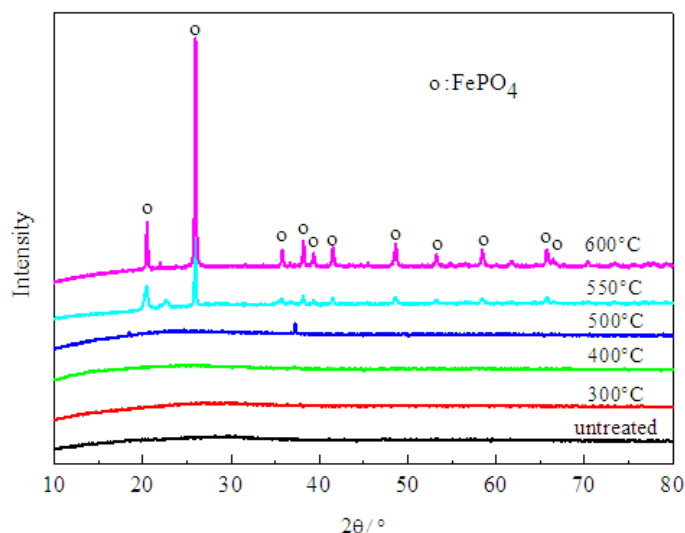
Figure 2. XRD patterns of as obtained powders calcined at different temperatures in air

TG-DSC curves of the as-prepared precipitate at a heating rate of $10\,^{\circ}$C/min are illustrated in Figure 3. It can be seen from the TG curve that there is a weight loss between 50 and 500 $^{\circ}$C, which is attributed to the elimination of crystallisation water. The dehydration process can be divided in two ranges of 50-200 and 200-500 $^{\circ}$C. The corresponding weight loss is 22.00 and 4.80% by mass, which corresponds to 2.50 and 0.56 mol of water, respectively. The total weight loss of 26.80% corresponds to 3.06 mol of water, which is close to the theoretical value for $FePO_4 \cdot 3H_2O$ (26.39%, $3H_2O$). Two endothermic effects are displayed in the DSC curve at 129 and 380 $^{\circ}$C, owing to the dehydration of water molecules. Three exothermic effects at 517, 533 and 548 $^{\circ}$C without appreciable weight loss are attributed to the transformation from amorphous to pure crystalline phase of $FePO_4$. These exothermic effects likely indicate three-step structural transformation of the FePO framework [9].
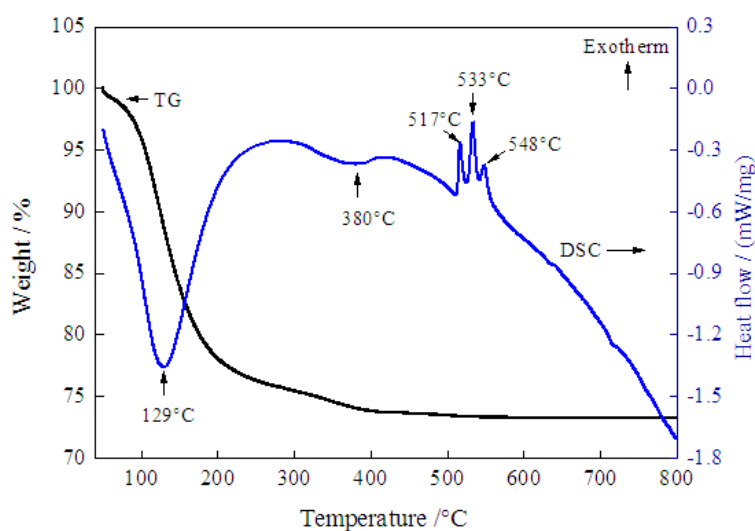

Figure 3. TG-DSC curves of the particles produced by ISR

The hydrated water molecules were identified by FT-IR spectra as shown in Figure 4. The total characteristics of the as-prepared precipitate are similar to the results reported in the literature [9-12,15]. A strong wide band in the $3000-3500$ cm^{-1} region is attributed to the stretching vibration of OH groups of H_2O molecules. A medium intensity absorption peak at around 1630 cm^{-1} is attributed to the water bending vibration. A strong and broad absorption peak at 1030 cm^{-1}, and another medium peak at 540 cm^{-1} are due to O-P and O-P-O bending vibration, respectively. As it can be seen the water bands are weaken when the as-prepared precipitate was calcined at 480 °C for 5 hours in air. But, these water bands disappear in FT-IR spectra of its lithiation product (heating treatment at 700 °C in N_2), which supports agreement with the thermal analysis results.
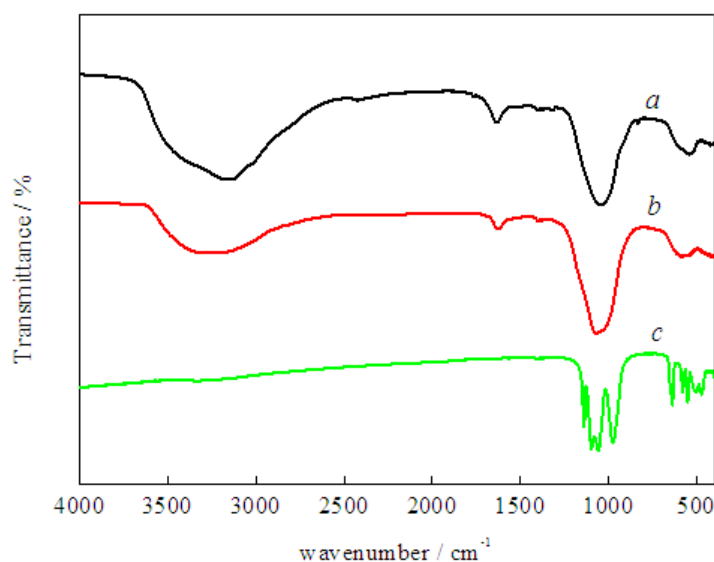

Figure 4. FT-IR spectra of *a* :as-prepared precipitate; *b*: dehydration product of *a*; *c*: lithiation product of *b*.

Based on the results of XRD, TG-DSC, and FT-IR measurements mentioned above, the chemical formula of the synthesized product is $FePO_4 \cdot 3H_2O$.

3.2. Particle size distribution

For sake of comparison, a conventional stirred tank reactor (STR) with an effective volume of 1.0 L as shown in Figure 5 was also employed to perform the synthesis of the precursor through the reaction between ferric nitrate and phosphoric acid. Under the conditions as follows, the reaction temperature of 50 °C, reactant initial concentration of 1.0 mol/L, solution pH of 2.30, and stirring speed of 1500 rpm. The yellowish-white precipitates form immediately, indicating the reaction rate is very rapid. Whereas the particles will grow by the aggregation of primary small particles and the size should increase with the increasing residence time of particles in the reactor. Because the effective

volumes of ISR and STR are different, the residence time must be different at the same flow rate. Based on these considerations, the space time was used as governing variable.
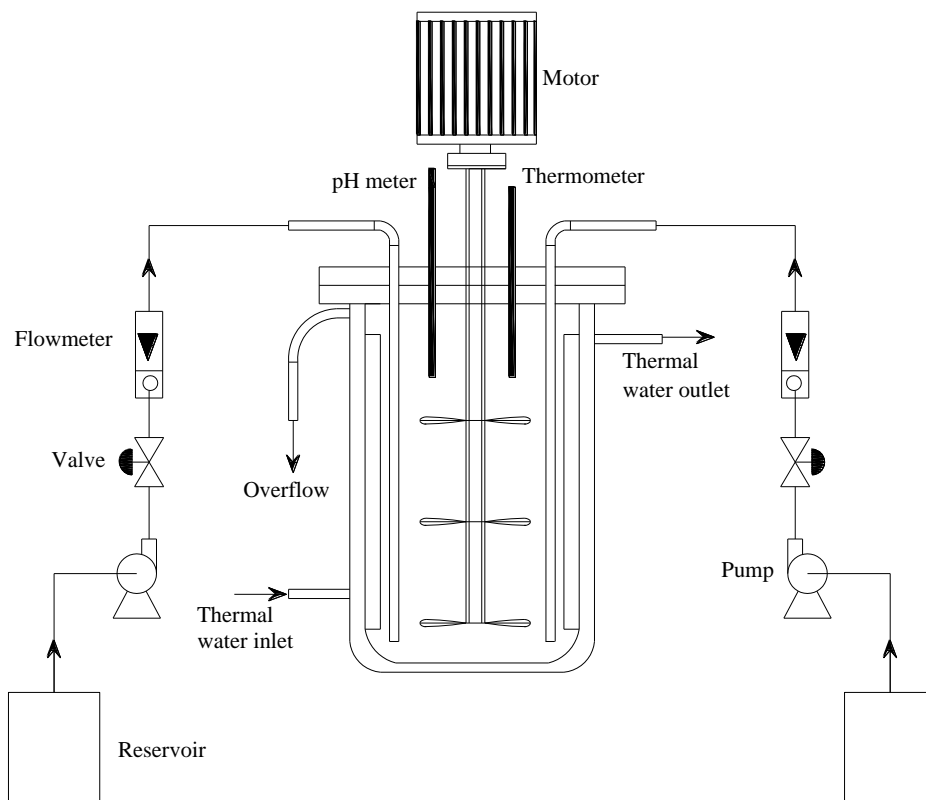

Figure 5. Schematic view of stirred tank reactor equipment

The space time, τ, which is inversely proportional to the flow rate

$$\tau = \frac{V_R}{q_V} \qquad (1)$$

where V_R is the effective volume of the reactor, L; q_V is the flow rate.

At the various τ and the same other conditions above mentioned, the cathode material precursor FePO$_4$·3H$_2$O was prepared by ISR and STR, respectively. The size and PSDs of FePO$_4$·3H$_2$O produced by the two reactors are presented in Figure 6 and Figure 7, respectively. It is clear from the two Figures that the particles prepared using ISR have a much narrower PSD and a much smaller average size than those prepared using STR, even at the same τ. Furthermore, the former has a single distribution, while the latter has a multi-distribution. These phenomena resulted from the mixing effect of the materials in the reactor, which can be investigated by the RTD and micromixing measurements.

The SEM micrographs of FePO$_4$·3H$_2$O produced by the two reactors are shown in Figure 8. The precipitates prepared using both ISR and STR are spherical shape. However, it is further confirmed that the particles produced by ISR are much smaller than that produced by STR.
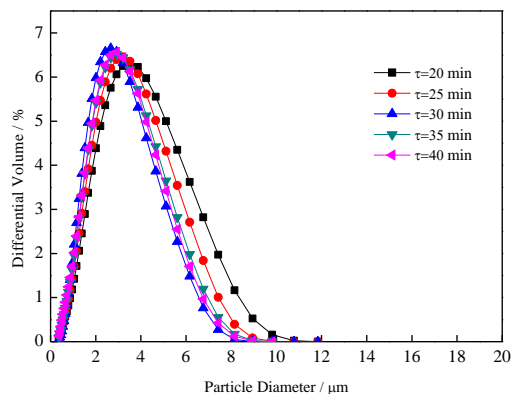
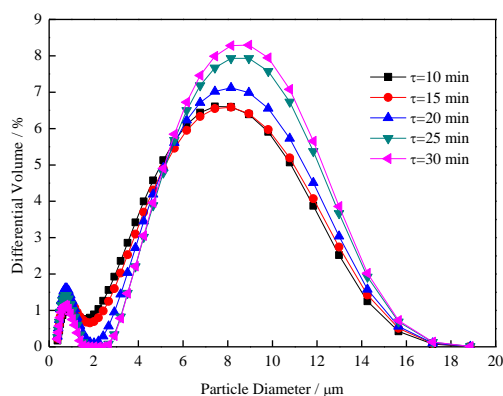**Figure 6.** Particle size distributions of FePO$_4$·3H$_2$O prepared by ISR at different space times

Figure 7. Particle size distributions of FePO$_4$·3H$_2$O prepared by STR at different space times

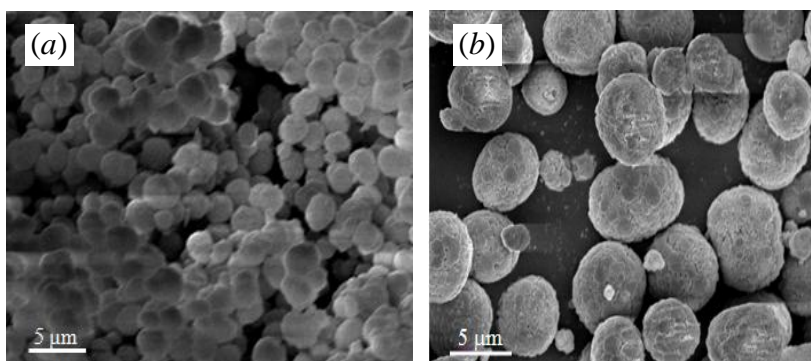**Figure 8.** SEM images of FePO$_4$·3H$_2$O prepared by ISR (*a*) and STR (*b*)

3.3. Flow behavior of reactor

In order to understand the difference of flow behavior between ISR and STR, residence time distributions in the two reactors were determined via the electro-conductivity input-response technique with KCl solution as the tracer at room temperature.

The RTDs in the two reactors are shown in Figure 9. It should be noted that the residence time in ISR is longer than that in STR by about 3 times at the same flow rate. The statistical characteristic values are listed in Table 1. The values of mean residence time, t_{m}, and variance, σ_{t}^2, in ISR are also greater than that in STR, which is because the effective volume of the former is much larger than that of the latter. The dimensionless variance, σ_{θ}^2, reflects the degree of backmixing. The smaller σ_{θ}^2 is, the lower degree of backmixing, and the narrower RTD of materials in reactor. As it can be seen the high similarity of σ_{θ}^2 values (~0.66) at the same flow rate indicates that the two reactors almost possess the same degree of backmixing. Micromixing effects in the two reactors, therefore, were investigated in order to further probe the cause of the superiority of ISR.
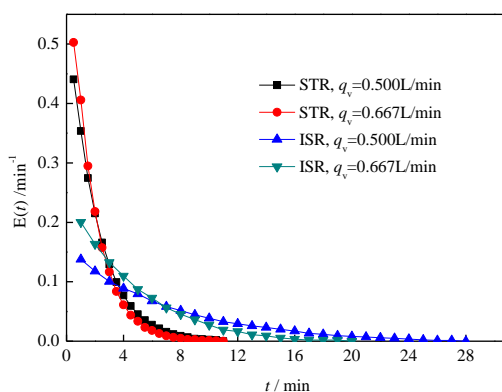

Figure 9. RTDs in ISR and STR at different flow rate

Table 1. Characteristic values of RTDs in ISR and STR

	q_{v}=0.500L/min			q_{v}=0.667L/min		
	t_{m}/min	σ_{t}^2/ min^2	σ_{θ}^2	t_{m}/min	σ_{t}^2/ min^2	σ_{θ}^2
ISR	6.668	30.007	0.675	4.410	12.624	0.649
STR	2.157	3.113	0.669	1.864	2.309	0.664

3.4. Micromixing effect

Bourne reaction scheme[16, 17], namely, the azo coupling reactions between α-naphthol (A) and diazotized sulfanilic acid (B) to produce monoazo dye (R) and bisazo dye (S) has been widely accepted and applied for the characterization of micromixing, for which the rate constants have been determined [18, 19]. The relative amount of S formed can be used to characterize micromixing effect. For this purpose the selectivity of S, X_{S}, is defined as

$$X_{\mathrm{S}} = \frac{2c_{\mathrm{S}}}{2c_{\mathrm{S}} + c_{\mathrm{R}}} \qquad (2)$$

The larger the value for X_S, the higher is the segregation degree, indicating the micromixing effect is worse.

Taking into account the impact of the energy dissipation on the mixing effect, the specific effective power, P_{eff}, is taken as the basis for comparison and is defined as

$$P_{eff} = (P - P_0)/V_R \qquad (3)$$

where P is the power practically inputted into the filled reactor by the propellers; while P_0 is that inputted into the empty reactor.

The experiments were carried out in the mode of continuous operation. The initial concentration ratio of A to B is 1.4 in order to ensure B being the limiting component. The samples are analyzed with a spectrophotometer (722S, Shanghai). The absorbance of each sample was measured at an interval of 10 nm in the wave length ranged from 460 to 600 nm, and the concentrations c_R and c_S in the sample mixtures were determined by a linear regression with the specific molar absorbance measured.

All the operating conditions in the two reactors are the same except P_{eff}. Figure 10 illustrates the data measured for the segregation indexes in ISR and STR, respectively. It is very clear that the micromixing effect of ISR is much better than that of STR. Hence, the $FePO_4 \cdot 3H_2O$ precursor produced by ISR possesses finer size and narrower PSD, since ISR with much better micromixing can provide a more homogeneously supersaturated environment before the onset of any nucleation [19].
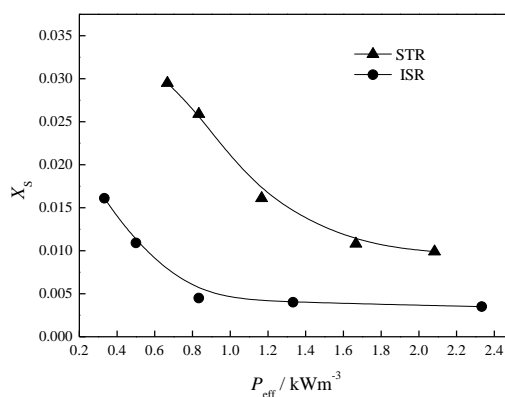

Figure 10. Influence of specific effective power on X_S in ISR and STR

3.5. Electrochemical characterization

Using the solid-state reaction, the cathode material $LiFePO_4/C$ was further prepared from the precursor $FePO_4$ after heat treatment at 550 °C for 5 hours. Coating carbon on the $LiFePO_4$ particle surface can effectively improve its electronic conductivity. The mixture with the molar ratio of $FePO_4:Li_2CO_3:sucrose = 1:0.52:0.1$ was ground by ball milling (480 rpm, agate balls) for 2 hours in water. After the ball milling, the mixture was dried at 80 °C for 6 hours. Finally, the cathode material

LiFePO$_4$/C was prepared by sintering the mixture in a tube furnace at 700 $^{\circ}$C at a heating rate of 3 $^{\circ}$C/min for 16 hours under N$_2$ atmosphere.

The working electrode was prepared by grinding LiFePO$_4$/C, carbon black, and PTFE at a weight ratio of 8:1:1, and then drying in vacuum at 120 $^{\circ}$C for 12 hours. The CR2032 coin cells were assembled in an Ar-filled glove-box with moisture and oxygen contents below 2 ppm, using lithium metal foil as the counter electrode. The electrolyte was 1 M LiPF$_6$ in EC/DEC/DMC (1:1:1 by volume). A Celgard 2400 microporous polyethylene film was used as separator. The assembled cells were charged and discharged using a LAND system at various rates with voltage ranging 2.5-4.2 V (vs. Li/Li$^+$) at room temperature. All the working electrodes were prepared in the same procedures except the precursor FePO$_4$.

Figure 11 shows the cycling profiles of the samples under room temperature at the currents of 0.1, 0.5, 1, and 2 C rates, respectively. The structural rearrangement on Li-ion extraction/reinsertion in LiFePO$_4$ is small [20]. Therefore, it can be seen from Figure 11 that both samples present excellent electrochemical cycling properties. Nevertheless, it can also be observed that the LiFePO$_4$/C obtained from FePO$_4$ produced by ISR exhibits higher specific capacity than that produced by STR. The path length for lithium ion diffusion from inner to surface of particles is longer for larger particles than for smaller particles. Decreasing particle size and obtaining uniform size distribution by optimizing synthesis processes to shorten the distance of the solid state diffusion of Li$^+$ within the electrode materials were proposed to overcome the ionic transport limitation [21]. On the other hand, smaller particles have greater specific surface area and can provide much more interface of electrochemical reaction. As a result, the electrochemical reaction is promoted by not only shorter diffusion path but also greater reaction interface. Since the LiFePO$_4$/C obtained from FePO$_4$ produced by ISR has smaller size and narrower PSD than that produced by STR, it would seem reasonable that Li-ion extraction/reinsertion will be more efficient and result in higher capacity. In addition, along with the raise of the charge/discharge rate, the advantage of the sample from ISR becomes more obvious. Thus, the electrochemical performances of LiFePO$_4$ could be effectively enhanced by using the precursor FePO$_4$ with smaller particle size and narrower PSD, due to the effective increase of Li-ion diffusion capability and expansion of the interface of electrochemical reaction.

Further investigation on the electrochemical performances, such as cyclic voltammograms at various scan rates, higher rate capability, and low temperature performances, will be undertaken.
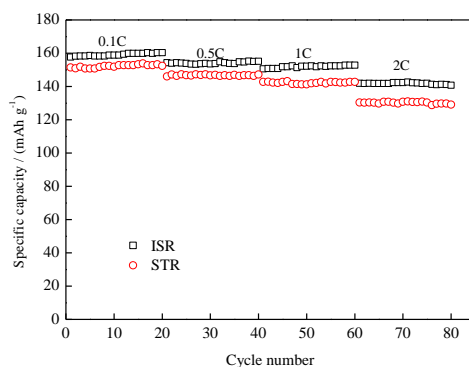

Figure 11. Cycle performance of the LiFePO$_4$/C samples at 0.1C, 0.5C, 1C, 2C rates

4. CONCLUSION

Ferric phosphate hydrate, one of the most important precursor of lithium iron phosphate, was prepared by performing the reaction between $Fe(NO_3)_3 \cdot 9H_2O$ and H_3PO_4 with aqueous ammonia as the precipitating agent in an improved ISR. The chemical formula for the synthesized product was identified to be $FePO_4 \cdot 3H_2O$ by the XRD, TG-DSC and FT-IR measurements. After calcining at 600 $^{\circ}$C for 5 hours, the amorphous $FePO_4 \cdot 3H_2O$ particles transform to pure crystalline phase of anhydrous $FePO_4$. The $FePO_4 \cdot 3H_2O$ prepared by ISR has much finer size and narrower PSD than that by STR. The degree of backmixing in ISR is similar to that in STR. However, micromixing effect in ISR is much better than that in STR, which leads to ISR can produce $FePO_4 \cdot 3H_2O$ with finer size and narrower PSD. The cathode material $LiFePO_4/C$ obtained from the precursor $FePO_4 \cdot 3H_2O$ prepared by ISR possesses better electrochemical performance.

References

1. A.K. Padhi, K.S. Nanjundaswamy, J.B. Goodenough. *J. Electrochem. Soc.*, 144(1997) 1188.
2. H.C. Wong, J. R. Carey, J. S. Chen. *Int. J. Electrochem. Sci.*, 5(2010)1090.
3. Y. Li, S. Zhao, C. Nan. *J. Alloy. Compd.*, 509(2011)957.
4. N. Jayaprakash, N. Kalaiselvi, P. Periasamy. *Int. J. Electrochem. Sci.*, 3(2008)476.
5. T. Honma, K. Hirose, T. Komatsu, T. Sato, S. Marukane. *J. Non-Cryst. Solids*, 356(2011)3032.
6. S. Yang, X. Zhou, J. Zhang. *J. Mater. Chem.*, 20(2010)8086.
7. C. Hu, H. Yi, H. Fang, B. Yang, Y. Yao, W. Ma, Y. Dai. *Int. J. Electrochem. Sci.*, 5(2010)1457.
8. J. Gao, J. Li, X. He, C. Jiang, C. Wan. *Int. J. Electrochem. Sci.*, 6(2011)2819.
9. S. Scaccia, M. Carewska, A.D. Bartolomeo, P.P. Prosini. *Thermochim. Acta.*, 383(2002)145.
10. B. Boonchom, C. Danvirutai. *Ind. Eng. Chem. Res.*, 46(2007)9071.
11. B. Boonchom, S. Puttawong. *Physica B.*, 405(2010) 2350.
12. E. Pierri, D. Tsamouras, E. Dalas. *J. Cryst. Growth*, 213(2000)93.
13. Y. Wu, Y. Xiao, Y. Zhou. *Chinese J. Chem. Eng.*, 11(2003)420.
14. R. Chi, Z. Xu, Y. Wu, C. Wang. *J. Rare Earth.*, 25(2007)42.
15. K. Kandori, T. Kuwae, T. Ishikawa. *J. Colloid. Interf. Sci.*, 300(2006)225.
16. J. R. Bourne, F. Kozichi, P. Rys. *Chem. Eng. Sci.*, 36(1981)1643.
17. J. R. Bourne. *Chem. Eng. Commun.*, 16(1982)79.
18. J. R. Bourne, C.Hilber, G. Tovstiga. *Chem. Eng. Commun.*, 37(1985) 293.
19. A. J. Mahajan, D. J. Kirwan. *AIChE. J.*, 42(1996)1801.
20. A.S. Andersson, B. Kalska, L. Haggstrom, J.O. Thomas. *Solid State Ionics*, 130(2000)41.
21. J. Ren, W. Pu, X. He, C. Jiang, C. Wan. *Ionics*, 17(2011)581.